Biochimica et Biophysica Acta 1788 (2009) 2497–2508

Contents lists available at ScienceDirect

Biochimica et Biophysica Acta

journal homepage: www.elsevier.com/locate/bbamem

Conformational and dynamics simulation study of antimicrobial peptide hedistin—heterogeneity of its helix–turn–helix motif

Guohua Xu [a], Min Wu [a], Lin Wang [a], Xu Zhang [b], Shufen Cao [a], Maili Liu [b], Yanfang Cui [a,*]

[a] Key Laboratory of Pesticide and Chemical Biology, Ministry of Education, Central China Normal University, Wuhan 430079, PR China
[b] State Key Laboratory of Magnetic Resonance and Atomic and Molecular Physics, Wuhan Institute of Physics and Mathematics, The Chinese Academy of Sciences, Wuhan 430071, PR China

ARTICLE INFO

Article history:
Received 18 May 2009
Received in revised form 27 September 2009
Accepted 2 October 2009
Available online 9 October 2009

Keywords:
Antimicrobial peptide
Hedistin
Nuclear magnetic resonance
Helix–turn–helix motif
Molecular dynamics simulation
Heterogeneity

ABSTRACT

Hedistin is an antimicrobial peptide isolated from the coelomocytes of *Nereis diversicolor*, possessing activity against a large spectrum of bacteria including the methicillin resistant *Staphylococcus aureus* and *Vibrio alginolyticus*. The three-dimensional structure of hedistin in both aqueous solution and deuterated dodecylphosphocholine (DPC) micelles was examined using circular dichroism (CD) and nuclear magnetic resonance (NMR) techniques. And, the early events of the antibacterial process of hedistin were simulated using palmitoyl-oleoyl-phophatidylcholine (POPC) lipid bilayers and molecular dynamics (MD) simulation methods. Hedistin lacks secondary structure in aqueous solution, however, in DPC micelles, it features with a heterogeneous helix–turn–helix moiety and exhibits obvious amphipathic nature. The turn region (residues Val9–Thr12) in the moiety is a four-residue hinge, lying in between the first N-terminal α-helix (residues Leu5–Lys8) and the second α-helix (residues Val13–Ala17) regions and causing an ~120° angle between the axes of the two helices. The segmental and nonlinear nature of hedistin structure is referred to as the heterogeneity of its helix–turn–helix motif which was found to be corresponding to a kind of discrete dynamics behavior, herein coined as its dynamical heterogeneity, at the early stage (0–50 ns) of the MD simulations. That is, the first helix segment, prior to (at 310 K) or following (at 363 K) the second helix, binds to the lipid head-group region and subsequently permeates into the hydrophobic lipid tail region, and the hinge is the last portion entering the lipid environment. This result implies that hedistin may adopt a "carpet" model action when disrupting bacterial membrane.

1. Introduction

Antimicrobial peptides (AMPs), the first line of defense in the innate immune system of all organisms, are considered as prospective antibiotic agents as they exhibit a broad spectrum of antimicrobial activity and are believed to be difficult for bacteria to develop resistance [1–3]. Since their discovery in the early 1980s, continuing exploration of AMPs has been fueled by the fact that antibiotic resistant pathogenic bacteria such as methicillin resistant *Staphylococcus aureus* (MRSA) and vancomycin resistant enterococci (VRE) are emerging with increasing frequency [4–7]. Aquatic invertebrate is of an intensive source of AMPs as they use their innate immune system as principal defense against potential pathogens due to the lack of acquired immunity with a system of antibodies diversification while living in microbe laden environment [8]. A variety of AMPs from aquatic invertebrates have been described, and they include the cystein-rich peptides of myticins and mytilins from mussels [9], and tachyplesins and tachystatins from horseshoe crabs [10], the proline and cystein-rich peptides of penaeidins from shrimp [11] and the α-helical peptides of clavanins, styelins from ascidians [12,13]. Further study of these AMPs will advance our understanding of innate immunity, facilitate the development of aquaculture and help the design of new antibiotics manifesting broad-spectrum antibacterial activity.

Among those AMPs, hedistin was isolated most recently from the coelomocyte of *Neries diversicolor* [14]. As a kind of marine annelid, *N. diversicolor* lives in the mud of marine-terrestrial interlaced zones rich in microorganisms and a large number of toxic agents. It is accordingly thought to possess special detoxicative ability and draw research interests from ecologists [15]. Hedistin was identified by Tasiemski and co-workers [14] as the first brominated AMPs from marine annelid though bromination was tested and found to be not affecting its antimicrobial activity. Its gene was constitutively expressed in NK cells like and the peptide was released into the

Abbreviations: DPC, dodecylphosphocholine; CD, circular dichroism; NMR, nuclear magnetic resonance; MD, molecular dynamics; AMPs, antimicrobial peptides; MRSA, methicillin resistant *Staphylococcus aureus*; VRE, vancomycin resistant enterococci; POPC, palmitoyl-oleoyl-phophatidylcholine; SDS, sodium dodecyl sulphate; DQF-COSY, double-quantum filtered correlation spectroscopy; TOCSY, total correlation spectroscopy; NOESY, nuclear Overhauser effect spectroscopy; DSS, sodium 2, 2-dimethyl-2-silapentane-5-dulfonate salt; SPC, simple point charge; PME, Particle mesh Ewald; CSI, chemical shift index; DSSP, dictionary of secondary structure of proteins

* Corresponding author. Tel.: +86 0 27 6786 7885; fax: +86 0 27 6786 7961.
E-mail address: yfcui@mail.ccnu.edu.cn (Y. Cui).

0005-2736/$ – see front matter © 2009 Elsevier B.V. All rights reserved.
doi:10.1016/j.bbamem.2009.10.001

local environment upon bacterial challenges. It shows antibacterial activity to a broad spectrum of Gram-positive microorganisms including methicilin-resistant *S. aureus*, but it shows antibacterial activity to only one class of Gram-negative marine bacteria *Vibrio alginolyticus*. Hedistin exhibits very weak sequence similarities to other known peptides though it is cationic only consisting of 22 amino acids. Up to date, neither conformational information nor mechanism of action for hedistin has been proposed. To investigate the structure of hedistin and the mechanism of its antibacterial activity, the hedistin peptide with the bromotryptophan residues replaced by unmodified tryptophan residues was synthesized, and the structure was examined in both aqueous solution and mimetic membrane environment utilizing CD and NMR approaches in this study.

The obtained conformation knowledge of hedistin renders further exploration of its structure–function relationship at the atomic level using molecular dynamics (MD) simulation and this method has been extensively employed in revealing the action mechanism of antibacterial peptides [16–19]. Although it is believed that most membranelytic peptides play its lytic activity via peptide–lipid interactions rather than receptor-mediated recognition processes [20–22], and some action mechanism speculations such as toroidal pore model [23,24] and "carpet" model [25,26] have been proposed, the mechanism of action for many of these peptides remains unclear. The main purpose of our MD simulations of hedistin in water and at zwitterionic palmitoyl-oleoyl-phosphatidylcholine (POPC)/water interface is to address the early events in the process of the peptide interaction with bacterial membrane.

2. Materials and methods

2.1. Preparation of peptide sample

Hedistin (LGAWLAGKVAGTVATYAWNRYV-NH_2) was synthesized by the solid phase method at WuhanNewEast Biosciences Co., Ltd. The synthetic peptide was purified by reverse-phase high-pressure liquid chromatography (RP-HPLC). The purity of peptide was determined by analytical RP-HPLC and confirmed greater than 95%. The purified peptide was characterized by MALDI/TOF-MS. Perdeuterated dodecylphosphocholine (DPC) was purchased from Cambridge Isotope (Woburn, MA). DPC and sodium dodecyl sulphate (SDS) micelles were prepared according to the method presented by Choi et al. [27].

2.2. Antibacterial activity assays

Synthesized and purified hedistin powder was solved in double distilled water, resulting in a stock solution with hedistin concentration of 0.6 mg/mL. This stock solution was then filtered through a diameter ~0.22 μm Millipore filter, and subsequently diluted into three hedistin sample solutions with hedistin concentration of 0.3, 0.15, and 0.075 mg/mL, respectively. These three samples were used in the following described antibacterial activity assay, and three replicas of assay were made for each sample.

The antibacterial activity was evaluated using both standard and a slightly modified "agar well diffusion method" [28]. As for the latter method, briefly, 90 mm Petri dish received 10 mL of 0.7% agar in NB broth. After the agar hardened, a 200 μL aliquot of the bacteria containing 2×10^5 logarithmic-phase cells of *S. aureus* was dropped over center of the plate and spread evenly over the surface with a sterile, L-shaped glass rod. Wells (2 mm diameter) were punched in the plates using a sterile stainless steel borer, every well was filled with a 25-μL aliquot of the test sample. The plates were incubated overnight at 37 °C. If the sample examined had antimicrobial activity, a clear zone would be formed on the surface of the top agar representing inhibition of tested bacterial growth.

2.3. Circular dichroism spectroscopy

The samples for CD experiments were prepared by dissolving the peptide to the concentration of 100 μM in various solvents: 10 mM phosphate buffer (pH 7.0, 5.2), 7 mM SDS micelles (1: 70 peptide/SDS molar ratio, pH 7.0, 5.2), 15 mM SDS micelles (1:150 peptide/SDS molar ratio, pH 7.0, 5.2), 7 mM DPC micelles (1:70 peptide/DPC molar ratio, pH 7.0, 5.2). The CD spectra were measured using a Jasco J-810 spectropolarimeter (Tokyo, Japan) and using a 1 mm path-length cell. Each CD spectrum of the peptides was recorded in the 190–250 nm wavelength range, with 1 nm bandwidth. Three successive scans were added and averaged, followed by subtraction of the sample blank. All the samples were performed at 25 °C, except that the sample of the peptide in 7 mM DPC at 25, 37 °C, respectively. The CD intensity was expressed in terms of mean residue molar ellipticity $[\theta_m]$ (deg·cm^2·d-mol^{-1}) according to Eq. (1).

$$[\theta_m] = \theta_{mdeg} / lCN \quad (1)$$

Where θ_{mdeg} is the measured ellipticity in millidegrees, l is the cell path length in cm, C is the molar concentration of the protein or peptide, N is the number of residues in the peptide.

2.4. NMR spectroscopy

A peptide hedistin sample in the presence of DPC micelles consisted of 2.0 mM peptide and 140 mM deuterated DPC (d-38) in 0.6 mL of H_2O/D_2O (90%/10%, v/v) at pH 5.2. In the aqueous sample, 2.0 mM peptide hedistin was dissolved in 0.6 mL H_2O/D_2O (90%/10%, v/v) at pH 5.2. All one-dimensional and two-dimensional NMR spectra including phase-sensitive double-quantum filtered correlation spectroscopy (DQF-COSY) [29], total correlation spectroscopy (TOCSY) [30] and nuclear Overhauser effect spectroscopy (NOESY) [31] of the peptide in aqueous sample and DPC micelles were recorded either on Varian INOVA 600 or Bruker Avance 800 spectrometer (operating at either 600.16 or 800.13 MHz) at the temperature of 25 and 37 °C, respectively. All two-dimensional (2D) NMR data were obtained in the phase-sensitive mode using the TPPI method [32]. Sodium 2, 2-dimethyl-2-silapentane-5-sulfonate salt (DSS) was used as an external chemical shift reference. Water suppression was achieved using the WET [33] or WATERGATE [34] method. All 2D spectra were collected with 32 or 64 transients, 512 to 1024 data points in F1 and 2048 data points in F2. TOCSY spectra were acquired using the MLEV-17 pulse sequence [35] at spin-lock periods of 60, 80, and 100 ms. NOESY spectra were acquired using mixing times of 80, 150 and 200 ms.

2.5. Spectra analysis and structure calculation

All NMR data were processed with NMRPipe [36] and analyzed using SPARKY software [37]. Integrated NOE peak volumes on the 80 ms NOESY spectra were converted into distance constraints and divided into three classes: strong, medium, and weak, with the distance ranges of 1.8–2.7, 1.8–3.5, and 1.8–5.0 Å, respectively [38]. Standard pseudoatom corrections were applied to the non-stereo-specifically assigned restraints [39], and an additional 0.5 Å was added to the upper bounds for the NOEs involving methyl group [40].

Structure calculations were performed with a torsion angle molecular dynamics protocol using Xplor-NIH software (version 2.19) [41]. The torsion angle molecular dynamics algorithm starts from an extended strand conformation and proceeds in four stages: high-temperature torsion-angle molecular dynamics, slow-cooling torsion-angle molecular dynamics, cartesian molecular dynamics, and conjugate gradient minimization. A total of 100 structures were obtained and then 20 of them with lowest-energy structures were selected for further analysis. The MOLMOL [42] and PyMOL [43]

programs were used for final structure analysis and structure presentation. The stereochemical quality of the lowest energy structures was analyzed with PROCHECK [44].

2.6. Molecular dynamics simulations

All molecular dynamics simulations were performed using the GROMACS package (version 3.3.1) [45]. Molecular graphics images were generated using PyMOL [43]. The GROMOS force field was used for the peptide, and the initial POPC lipid bilayer structure (popc.pdb) and the modified GROMOS parameter files (lipid.itp and popc.itp) for lipids were downloaded from http://moose.bio.ucalgary.ca/download.html [46]. The simple point charge (SPC) water model was used for all simulations. All the simulations were performed in the NPT ensemble using periodic boundary conditions. The LINCS algorithm was used to restrain bond lengths [47]. Long range electrostatic interactions were calculated by using the Particle mesh Ewald (PME) method with a 1 nm cutoff for the real space calculation [48]. A cutoff of 1.2 nm was used for the van der Waals interactions. The time step for integration was 2 fs, and the coordinates and velocities were saved every 1 ps. The resulted dynamical trajectory was checked using VMD [49].

2.6.1. The simulation of hedstin in water environment

The simulation of peptide in water was performed by solvating the hedistin molecule in a cubic box of volume 125 nm^3 (5 nm× 5 nm× 5 nm) with 4014 waters. Two counter ions (Cl^-) were added to make the system electroneutral. The pressure was maintained at 1 atm by isotropic coupling to a Berendsen barostat and the temperature was maintained at 300 K by coupling to a Berendsen thermostat [50]. The time scale of the simulation was 70 ns.

2.6.2. The simulation of hedistin at the POPC/water interface

The initial downloaded POPC lipid bilayer system consists of 128 POPC lipids and 2460 water molecules. Additional 3639 water molecules were added to the system to enable larger distances between the periodic images of the lipid leaflets in the z-direction (direction perpendicular to the lipid–water interface). According to Kandasamy's method [51], this system was first equilibrated for 10 ns in the NPT ensemble. Then, hedistin was placed in the water phase, close to the POPC/water interface, with the hydrophilic part of amphipathic helix facing the lipid/water interface. Two counter ions (Cl^-) were added to make the system electroneutral. The pressure was maintained at 1 atm by isotropic coupling to a Berendsen barostat [50], and the temperature was maintained at 310 K and 363 K by coupling to a Berendsen thermostat [50], respectively. The simulations were performed for 50 ns at 310 K and 363 K, respectively.

3. Results

3.1. Antibacterial activity

The purity of the synthesized peptide has been determined higher than 95% using analytical RP-HPLC and the correctness of the synthesized peptide has been demonstrated using MALDI/TOF-MS (data not shown). To demonstrate the antibacterial activity of the synthesized hedistin, an antibacterial activity experiment was performed. As Tasiemski and co-workers [14] have assessed the MIC of native and synthesized hedistin against a large spectrum of Gram-positive and Gram-negative bacteria, it is mainly for the validating purpose that the antimicrobial activity evaluation of our synthesized hedistin was carried out using both standard and a slightly modified "agar well diffusion method." The two methods produced almost the same results. Fig. S1 (supplementary data) shows the antimicrobial assay of hedistin at various concentrations against the tested bacterium *S. aureus* using the modified "agar well diffusion method." Clear zones were found on the surface of the top agar, for hedistin at (B) 0.3 mg/mL (C) 0.15 mg/mL (D) 0.075 mg/mL, demonstrating that our synthesized hedistin effectively inhibited the growth of bacterium *S. aureus* in a concentration-dependent manner.

3.2. Circular dichroism analysis

In order to detect the secondary structure of hedistin under different conditions, CD spectra were recorded for the hedistin peptide in various environments including phosphate buffer, SDS and DPC micelles, with various pH values and temperatures (Fig. 1). The CD spectra for hedistin in phosphate buffer (at both pH 5.2 and pH 7.0) are characterized by a broad negative band at 200 nm, implying that no regular secondary structure exists under these conditions of mere aqueous solution. Whereas, in the presence of various amounts of SDS micelles (7 mM and 15 mM), hedistin gives rise to almost the same CD absorbance at 25 °C, and at both pH 5.2 and pH 7.0, exhibiting a maximum at 192 nm and two minima at 208 nm (helical ππ* transition) and 222 nm (helical nπ* transition), indicative of the presence of an α-helical conformation and no obvious variation of helicity with the change of pH or peptide/SDS ratio. Moreover, in the presence of DPC micelles (7 mM, pH 5.2; 7 mM, pH 7.0), the CD spectra of hedistin at 25 °C display similar profiles but more negative minima at both 208 nm and 222 nm compared to the situation of hedistin in SDS micelles, revealing that hedistin not only presents distinguished α-helical conformation in DPC micelles solution, but also exists with higher content of helicity compared to its status in SDS micelles environment. The helicity of hedistin in DPC micelles environment at pH 7.0 does not show distinct difference with the temperature varied between 25 and 37 °C (Fig. 1).

3.3. NMR spectra analysis and generation of conformation

Based on the above CD analysis, the detailed structure was studied using NMR method for samples of hedistin in phosphate buffer and in DPC micelles solution, respectively. It needs to be specified that the temperature of 37 °C was employed when the hedistin structure in DPC micelles was studied using NMR measurements just because higher temperature can shorten the molecular correlation time and narrow the resonances of hedistin.

3.3.1. Resonance assignment

The proton resonance assignment of hedistin in the presence of DPC micelles was made using the following procedures developed by

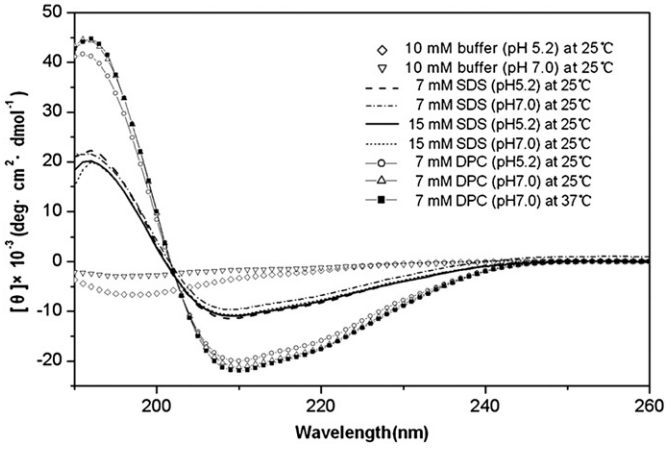

Fig. 1. Circular dichroism spectra of 100 μM peptide hedistin in various environments including phosphate buffer, SDS and DPC micelles. CD spectra were measured on a Jasco 810 spectropolarimeter (Tokyo, Japan) using a 1 mm path-length quartz cell. Each CD spectrum of the peptides was recorded in the 190–250 nm wavelength range, with 1 nm bandwidth. Three successive scans were added and averaged, followed by subtraction of the sample blank.

Wüthrich [52]. The spin system assignments of individual amino acid residues were identified mainly from TOCSY spectra. Gly, Ala, and Val residues were easily identified in the fingerprint region of the 80 ms TOCSY spectra (Fig. 2A). The ambiguous resonances of Trp, Asn, and Tyr residues and the overlapped residues, which were difficult to assign directly from TOCSY, were then completely identified with the assistance of NOESY and DQF-COSY spectra. The sequential assignments of residues were made by checking H_α/amide $d_{\alpha N}$ $(i, i+1)$ cross-peaks and further demonstrated by reference of amide d_{NN} $(i, i+1)$ cross-peaks as well as side-chain/amide $d_{\beta N}$ $(i, i+1)$ connectivities in the NOESY spectra (Fig. 2B).

Unlike in DPC micelles, all of the spin systems were very well-resolved in the TOCSY spectrum in aqueous solution. A similar assignment strategy was used for hedistin in aqueous environment. The fingerprint region of the 80 ms TOCSY spectrum and H_α/amide region of NOESY spectrum are shown in Fig. S2a and S2b (supplementary data), respectively. The complete proton resonance assignments of hedistin in aqueous solution and in DPC micelles are provided in Table S1 (supplementary data) and Table 1, respectively.

3.3.2. Analysis of chemical shift values

The elements of secondary structure were estimated on the changes in their H_α proton chemical shifts according to the method of

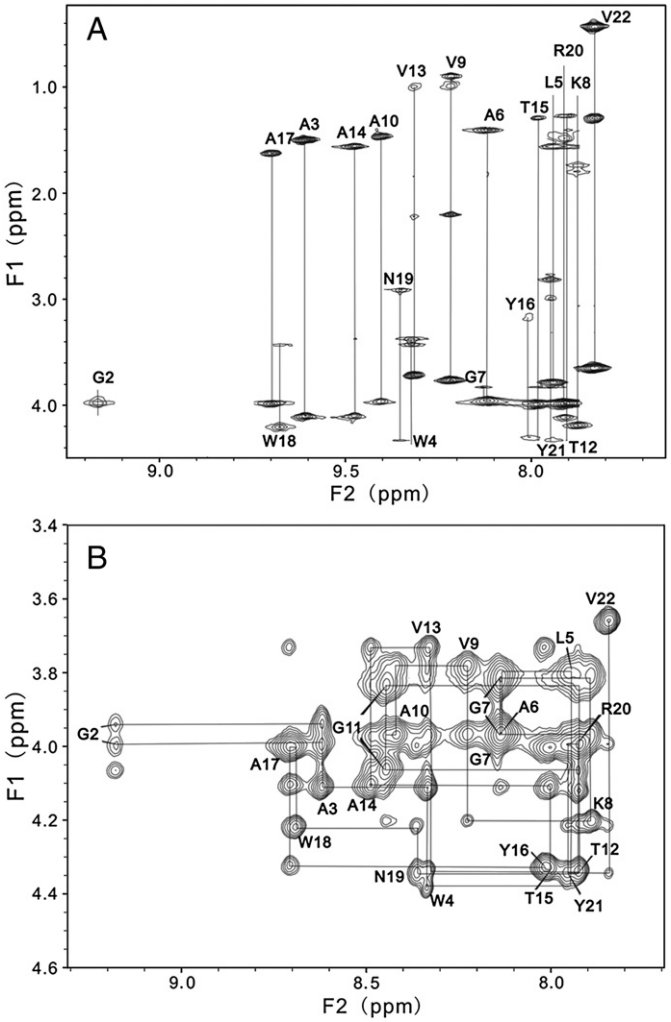

Fig. 2. (A) Partial 600 MHz ^{1}H NMR 2D TOCSY spectrum of 2 mM hedistin in 140 mM DPC micelles at 37 °C, pH 5.2. The spin systems of amino protons are designated by one-letter code, uppercase letters. (B) Partial 600 MHz ^{1}H NMR 2D NOESY (80 ms, mixing time) spectrum of 2 mM hedistin in 140 mM DPC micelles at 37 °C, pH 5.2. For the sake of clarity, only the intra-residue α-amide cross-peaks are labeled.

Table 1
Chemical shifts for hedistin in the presence of 140 mM DPC micelles.

Residue	NH	αH	βH	Others
Leu[1]		4.06	1.80, 1.80	γ:1.80; δ*:0.99, 0.97
Gly[2]	9.17	3.93, 3.98		
Ala[3]	8.61	4.10	1.51	
Trp[4]	8.33	4.38	3.41	HD1:7.43; HE3:7.51; HZ3:6.96; HH2:7.09; HZ2:7.54; HE1:10.71
Leu[5]	7.95	3.79	1.55	γ:1.47, δ*:0.87, 0.82
Ala[6]	8.12	3.95	1.41	
Gly[7]	8.13	3.96, 3.81		
Lys[8]	7.88	4.19	1.71, 1.77	γ*:1.23; 1.08; δ*:1.57; ε*:2.77, 2.88
Val[9]	8.22	3.77	2.20	γ*:0.84
Ala[10]	8.41	3.96	1.47	
Gly[11]	8.44	4.05, 3.82		
Thr[12]	7.91	4.32	4.11	γ*:1.27
Val[13]	8.32	3.72	2.24	γ*:1.00, 1.07
Ala[14]	8.48	4.10	1.56	
Thr[15]	7.99	4.32	3.99	γ*:1.29
Tyr[16]	8.01	4.32	3.19	δ*:7.12; ε*:6.80
Ala[17]	8.70	3.99	1.62	
Trp[18]	8.68	4.21	3.42	HD1:7.20; HE3:7.47; HZ3:6.98; HH2:7.15; HZ2:7.51; HE1:10.49
Asn[19]	8.35	4.34	2.71, 2.92	γNH2:7.58, 6.99
Arg[20]	7.91	3.99	1.49	γ*:1.15, 1.09; δ*:2.86, 3.04; HE:7.35; HH:6.87, 6.96
Tyr[21]	7.95	4.34	3.01, 2.80	δ*:6.98; ε*:6.74
Val[22]	7.83	3.65	1.29	γ*:0.43

"Chemical Shift Index (CSI)" developed by Wishart and co-workers [53]. A series of upfield H_α chemical shifts (at least three) relative to the random coil values indicate the presence of an α-helical structure and downfield shifts indicate the presence of β-sheets. The secondary shift values of hedistin in aqueous solution and in the presence of DPC micelles are presented in Fig. 3. As shown, in aqueous solution, only the secondary shift values for residues Thr15–Arg20 show successively negative values suggesting that hedistin shows helical propensity in this small region while residues Leu1–Ala14 exist in the disordered state. Whereas, in the presence of DPC micelles, continually negative (upfield) secondary shift values were observed for residues Ala3–Ala10 and Val13–Val22 suggesting that hedistin produces α-helical secondary structure in these two regions. Those largest negative chemical shift deviations measured for Leu5 (−0.38 ppm), Ala6 (−0.40 ppm), Ala10 (−0.39 ppm), Ala17 (−0.36 ppm), Trp18 (−0.49 ppm), Asn19 (−0.41 ppm), and Arg20 (−0.39 ppm) also indicate that all these residues belong to constrained parts of the molecule. Such a result of the existence of α-helical folding in the peptide from the chemical shift analysis shows consistency with that from the CD measurements. Noticeably, the chemical shift deviations for residues Ala3–Ala10 are prominently lower than that for residues Val13–Val22, indicating relatively lower helicity in the region of residues Ala3–Ala10.

3.3.3. Analysis of NOE connectivities

The pattern and size of sequential and medium-range interresidue NOEs extracted from NOESY experiment are important to characterize the secondary structure. The observed sequential and medium range interresidue NOE connectivities and their relative intensities of hedistin in the presence of DPC micelles are presented in Fig. 4. Closed boxes in the figure represent unambiguously assigned NOE connections while open boxes represent those that can not be unambiguously assigned due to spectral overlap but could exist according to their neighbouring assigned NOEs. The presence of $d_{\beta N}$ $(i, i+1)$ and d_{NN} $(i, i+1)$ connectivities reinforces the reliability of the resonance assignments. A group of unambiguous NOEs including $d_{\alpha N}$ $(i, i+3)$, Val13/Tyr16, Ala14/Ala17, $d_{\alpha N}$ $(i, i+4)$, Val13/Ala17, $d_{\alpha\beta}$ $(i, i+3)$, Val13/Tyr16, Ala14/Ala17 and sequential NOEs support the presence of an α-helical fold between residues Val13–Ala17. A group of unambiguous NOEs including $d_{\alpha N}$ $(i, i+3)$, Ala3/Ala6,

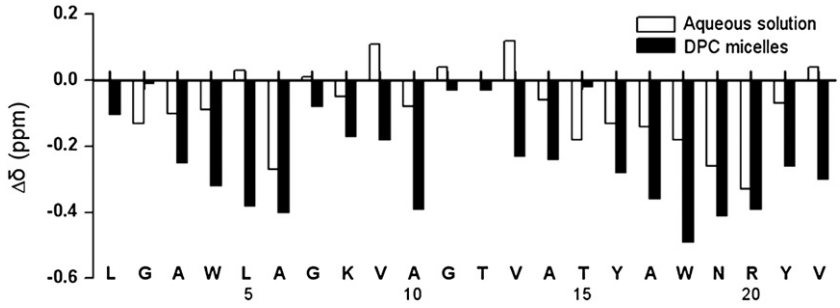

Fig. 3. Deviation of the H_α proton chemical shifts from random coil values for 2 mM hedistin in aqueous solution and in 140 mM DPC micelles. Closed boxes represent hedistin in 140 mM DPC micelles while open boxes in aqueous solution.

Trp4/Gly7, Leu5/Lys8, Ala6/Val9, $d_{\alpha\beta}$ (i, $i+3$), Ala3/Ala6, Leu5/Lys8, Ala6/Val9, and sequential NOEs support the presence of an α-helical fold between residues Ala3–Lys8. However, if NOEs from residues Ala3–Lys8 are compared with those from Val13–Ala17, it is apparent that none of unambiguous $d_{\alpha N}$ (i, $i+4$) NOEs were observed between residues Ala3–Lys8, indicating that more flexibility or looseness exists in the region of Ala3–Ala8. Obvious breaks of $d_{\alpha\beta}$ (i, $i+3$) NOEs, Lys8/Gly11 and Val9/Thr12, Gly11/Ala14 show interruption of helix between residues Val9–Thr12. But the existence of $d_{\alpha N}$ (i, $i+2$) NOEs, Val9/Gly11, $d_{\alpha N}$ (i, $i+4$), Val9/Val13, $d_{\alpha\beta}$ (i, $i+3$), Ala10/Val13, and $d_{\alpha N}$ (i, $i+3$), Ala10/Val13 (also shown as yellow dashed lines in Fig. 5), indicates that a kind of folding exists in the region Val9–Thr12. That means a turn exists in the region. In aqueous solution, although sequential NOEs connectivities were found (data not shown), characteristic NOEs indicative of secondary structure, including $d_{\alpha N}$ (i, $i+3$), $d_{\alpha N}$ (i, $i+4$), $d_{\alpha\beta}$ (i, $i+3$), $d_{\alpha N}$ (i, $i+2$), were not observed for hedistin. Hence, no calculation was further pursued for the structure of hedistin in aqueous solution. Such NOEs data display high consistency with the CSI data.

3.3.4. Generation of three-dimensional structure

Cross-peaks from the NOESY spectrum with mixing time of 80 ms were measured and subsequently divided into three classes, i.e. strong, medium, and weak, with distance ranges of 1.8–2.7, 1.8–3.5, and 1.8–5.0 Å, respectively. Those NOEs presenting obvious resonance overlap and those preventing unambiguous assignment were not used in structural calculation. As for those partly overlapped NOE peaks, such as those of Thr12HB/Thr15HN and Ala14HA/Thr15HN, the constraints were dealt with in a fairly larger range of 1.8–5.0 Å. A total of 388 distance restraints from those NOEs comprising 129 intra-residual, 120 sequential, 139 medium range restraints were employed to calculate the three-dimensional structures of hedistin in DPC micelles, using the torsion angle dynamics protocol of Xplor-nih [41]. A total of 100 structures were generated, of which 20 lowest energy structures were chosen for further analysis. The structure, as represented by an ensemble of the 20 lowest energy structures, is shown in Fig. 6 and the structural statistics is presented in Table 2. The quality of the structure has been checked with PROCHECK [44]. The Ramachandran plot for all 20 structures indicates that all the backbone dihedral angles (except for residues Gly and Pro) consistently lie in the α region of the plot, 77.4% of the backbone dihedral angles are found in the most favored regions, and none of them is found in the disallowed region. The generated structure coordinates in pdb format accompanied with the assigned chemical shift values and the utilized structure restraints can be accessed in BMRB-SMSdep database with the accession number of 20078.

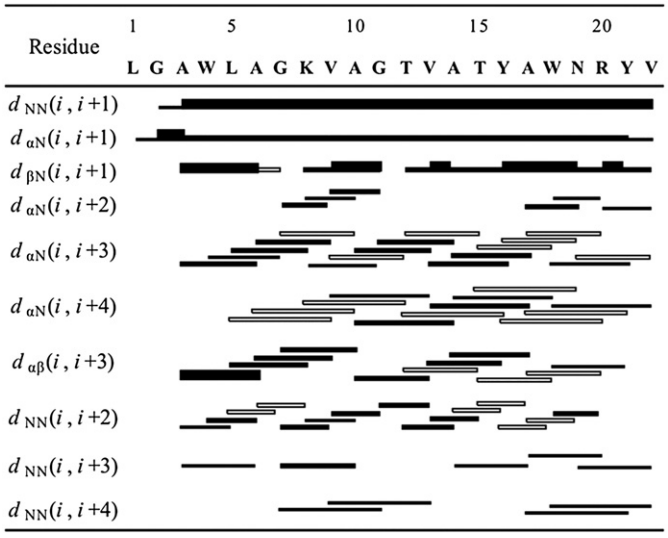

Fig. 4. Summary of inter-residue NOE connectivities found in NOESY spectrum of hedistin in 140 mM DPC micelles. Closed boxes represent unambiguously assigned NOE connections while open boxes represent those that can not be unambiguously assigned due to spectral overlap but could exist according to their neighbouring assigned NOEs.

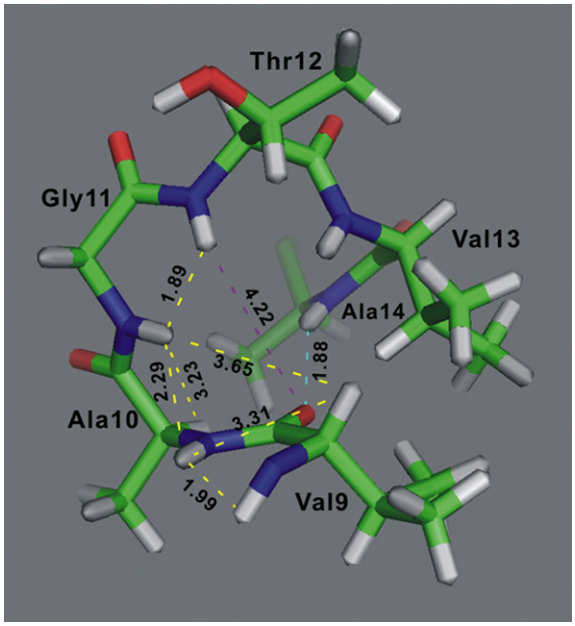

Fig. 5. Stick plot showing the turn formation for residues Val9–Thr12 (residues Val13 and Ala14 are also shown for sake of clarity). The nitrogen atoms are shown in blue, the hydrogen atoms in grey, and the oxygen atoms in red. Observed NOE connections that are critical to the folding pattern of this region are indicated using yellow dashed lines. Cyan dashed line connects CO oxygen of residue Val9 with NH hydrogen of residue Ala14, while purple dashed line shows the distance from the same oxygen atom to the NH hydrogen of residue Thr12. The distance values in angstrom (Å) are from conformation calculation results. This figure was generated using PyMOL [43].

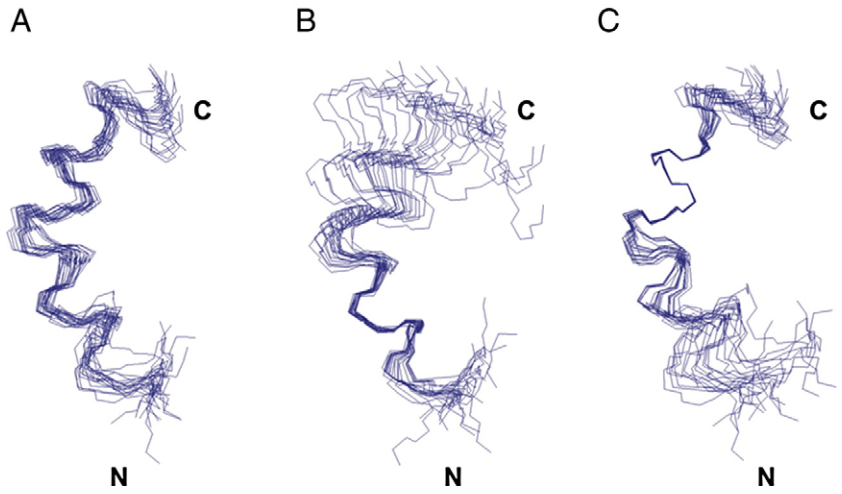

Fig. 6. Overlay of the 20 structures with lowest energy of hedistin in 140 mM DPC micelles. The structures were superimposed over the backbone atoms of all residues (A), residues Leu5–Lys8 (B), and residues Val13–Ala17 (C) with respect to the first structure, respectively. This figure was generated using MOLMOL [42].

The overall three-dimensional fold of hedistin in DPC micelles is depicted by three segments forming a helix–turn–helix conformation. The three regions contain a first N-terminal α-helix region (residues Leu5–Lys8), a turn (residues Val9–Thr12) and a second α-helix region (residues Val13–Ala17) (Fig. 6). The existence of the turn region between the two helices renders formation of an angle of ~120° between the axes of the two helices. This segmental and nonlinear conformation feature of hedistin is rather different from that of cationic linear AMPs where a single linear stretch of α-helix dominating the whole molecule. We refer to the in-segments and nonlinear structure feature of hedistin as its structural heterogeneity. As shown in Table 2, the structural statistics for hedistin in DPC micelles show that the pairwise root-mean-square-deviation (rmsd) calculated for backbone atoms of residues Leu5–Lys8 and Val13–Ala17 for all 20 structures is 0.30 ± 0.14 and 0.13 ± 0.05 Å, respectively. These low rmsd values show that the structures of the two segments are undoubtedly well defined, but residues Leu5–Lys8 are less folded than residues Val13–Ala17. However, the region encompassing residues Leu5–Ala17 exhibits an rmsd of 0.62 ± 0.28 Å for backbone atoms and 1.08 ± 0.29 Å for heavy atoms which is much larger than that of the other two regions, indicating that a wider range of conformers were sampled here possibly due to the existence of the turn structure adopted by residues Val9, Ala10, Gly11 and Thr12.

Table 2
Structural statistics for the 20 lowest-energy NMR structures determined for hedistin in 140 mM DPC micelles.

Experimental distance restraints	
Total	388
Sequential	120
Medium range	139
Intraresidue	129
Rmsd from experimental restraints	
Noe (Å)	0.0089 ± 0.0019
Rmsd from idealized geometry	
Bonds (Å)	0.00162 ± 0.000128
Angles (deg)	0.459626 ± 0.006906
Impropers (deg)	0.309049 ± 0.011035
Energies (kcal mol^{-1})	
E_{tol}	34.60 ± 1.29
E_{noe}	1.58 ± 0.71
E_{vdw}	9.31 ± 1.51
E_{ang}	19.90 ± 0.61
E_{bond}	0.90 ± 0.15
E_{imp}	2.91 ± 0.20
Ramachandran space (%)[a]	
Most favored	77.4
Additionally allowed	18.5
Generously allowed	4.1
Disallowed	0
Mean pairwise rmsd (Å)[b]	
Backbone atoms of all residues	1.52 ± 0.51
All heavy atom of all residues	2.08 ± 0.46
Backbone atoms of residues 5–8	0.30 ± 0.14
All heavy atom of residues 5–8	1.04 ± 0.39
Backbone atoms of residues 13–17	0.13 ± 0.05
All heavy atom of residues 13–17	0.66 ± 0.24
Backbone atoms of residues 5–17	0.62 ± 0.28
All heavy atom of residues 5–17	1.08 ± 0.29

[a] Calculated using PROCHECK [44].
[b] Calculated using MOLMOL [42].

The analysis of the calculated structures using the dictionary of secondary structure of proteins (DSSP) program [54] confirms that the region of residues Val9–Thr12 exists in a turn conformation, in accordance with what the NOEs observations imply for the region. Fig. 5 shows the measured distance values between some important atoms for the turn region Val9–Thr12 (extended to Ala14 for sake of clarity) as well as the observed NOE connections critical to the folding pattern of this region (yellow dashed lines). The distance (cyan dashed line) between CO group oxygen of residue Val9 and the NH group hydrogen of residue Ala14 is measured 1.88 Å and within the hydrogen bond length, while the distance (purple dashed line) between CO group oxygen atom of residue Val9 and the NH group hydrogen of residue Thr12 is measured 4.66 Å and out of the hydrogen bond length range. This hints that the turn region in hedistin molecule does not belong to any type of β-turn. A comparison of NOEs pattern for the region of Val9–Thr12 with that of a few turn types like turn I and turn II also proves that the turn in hedistin does not belong to any named turn types. The flexibility of Gly11 and the advantage of locating residue Thr12 at the hydrophilic side of the amphipathic dipole are most likely responsible for the formation of the turn encompassing residues Val9–Thr12.

Fig. 7 shows a ribbon diagram of the average structure of hedistin in DPC micelles displaying another herein determined feature of hedistin, which is its amphipathic property. As seen from the figure, the hydrophobic residues (Leu5, Ala6, Val9, Ala10, Val13, Ala14, Ala17, Trp18) colored in green are harbored in the concave portion of the peptide; while the charged residues (Lys8, Arg20) as well as polar residues (Thr12, Thr15, Asn19), all in blue, are positioned on the opposite face. The contact surface of the structure of hedistin in DPC micelles shown in Fig. 8 provides a clearer view for the amphipathic nature. In many cases, the amphipathic nature of an α-helical peptide is known to be important for membrane binding [55–57]. The amphipathic feature of hedistin in DPC micelles is also expected to be important to disrupt the microbial membrane integrity.

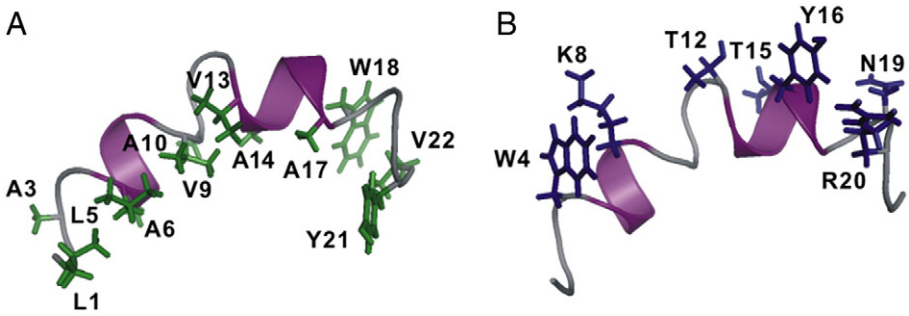

Fig. 7. Ribbon diagram of a representative structure of hedistin in 140 mM DPC micelles. The side chain atoms of hydrophobic amino acids are shown in green (panel A), and those of hydrophilic amino acids in blue (panel B). Noticeably, Residues Trp4 and Tyr16 are presented as hydrophilic residues while Tyr21 as hydrophobic residue. This figure was prepared using PyMOL [43].

As shown in Fig. 7, Trp4 is aligned on the hydrophilic side of the molecule rather than the hydrophobic side as expected, with its side chain staying close to that of hydrophilic Lys8. Five observed side chain NOEs (8HE1/4HE1, 8HE2/4HE1, 8HE1/4HZ2, 8HE2/4HZ2, 8HD1/4HE1, and 8HD2/4HE1) for residues Trp4 and Lys8 assured proximity of the side chains of the two residues, resulting in the side chain of Trp4 aligns on the hydrophilic side. However, as the resonance of NH_3^+ group protons of Lys8 did not appear in the NOESY spectrum, no direct NOEs for indole ring protons of Trp4 and NH_3^+ group protons of Lys8 were observed, causing lack of corresponding distance constraints. Therefore, the relative orientation of these two groups was not unambiguously determined. Our 20 lowest energy structure ensemble shows that, there are ~20% individual conformers adopting cation-π interaction favored orientation for these two inter-residue groups, as exampled in Fig. 9A and B (Fig. 9C and D are for the control purpose), even if no constraint was used for NH_3^+ protons of Lys8 and indole ring protons of Trp4. A cation-π interaction is that cations bind to the π face of an aromatic structure through a surprisingly strong, non-covalent force. The cation-π interaction can take place in either a parallel or a perpendicular, T-shaped orientation [58,59]. Conformers of hedistin with typical cation-π interaction observed do not show obvious lower energy compared with other conformers but more stable α-helical folding within residues Leu5–Lys8. That means, the cation-π interaction between residue Trp4 and Lys8 helps stabilize the local structure of the first α-helix of hedistin. A persistent cation-π interaction between residues Trp11 and Arg13 was for the first time observed in MD simulations of the indolicidin–lipid system, and validated to play an important role in stabilizing the structure of indolicidin in DPC micelles [58]. The possible cation-π interaction between residue Trp4 and Lys8 of hedistin, as stated, shows similarity to that between Trp11 and Arg13 of indolicidin peptide though there are three residues lying in between Trp4 and Lys8 in hedistin.

Residue Tyr16 is aligned on the hydrophilic side of the hedistin molecule while Tyr21 on the hydrophobic side, which is not surprising, considering the structure nature of tyrosine. Tyrosine has both a hydrophilic hydroxyl group and a hydrophobic aromatic ring in its side chain. Thus, on one hand, tyrosine is able to form hydrogen bond via its side-chain hydroxyl group with the head-group (phosphorylcholine) of DPC, assuring that tyrosine could stably exist in the hydrophilic side of the molecule; on the other hand, its hydrophobic aromatic ring is able to interact with the tail region of DPC via hydrophobic interaction, which leads tyrosine to exist in the hydrophobic side.

Since the conformation above examined is for the synthesized hedistin dissolved either in H_2O or in DPC micelles (see Materials and methods), the effect of salinity on the conformation and the

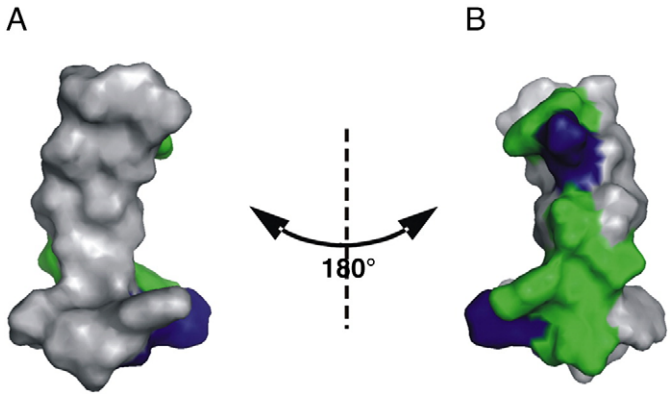

Fig. 8. Two-sided view of contact surface of structure of hedistin bound to DPC micelles. The hydrophilic amino acids without charge are shown in green, the two positively charged residues (Lys8 and Arg20) in blue and the hydrophobic residues in grey. Trp4 and Tyr16 are presented as hydrophilic residues and Tyr21 as hydrophobic residue. The amphipathic nature is quite obvious. This figure was generated using PyMOL [43].

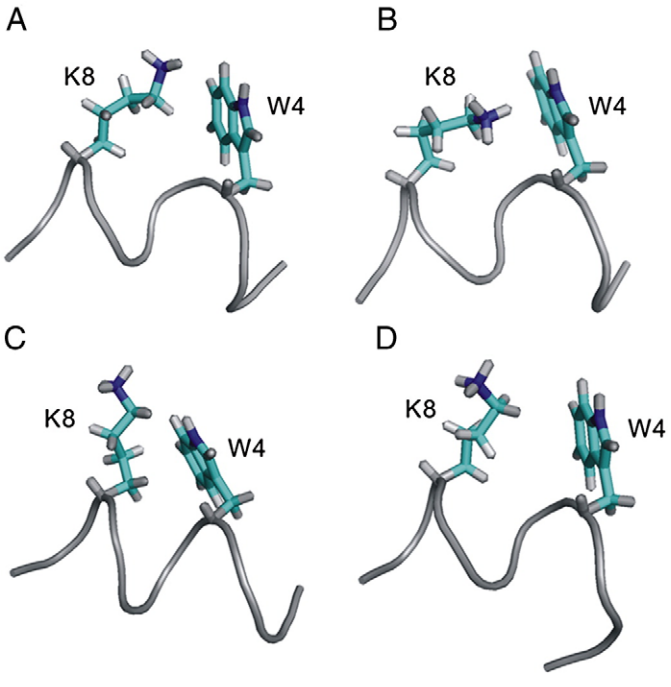

Fig. 9. Representative diagram for the presence of cation-π interaction formation (A and B) and the absence of cation-π interaction (C and D) between residues Trp4 and Lys8 in the calculated structure ensemble. Parts of main chains are displayed using grey tube. Side chains of residues Trp4 and Lys8 are presented using sticks. Side chain hydrogen, carbon, nitrogen atoms are colored grey, cyan and blue, respectively. The figure was generated using PyMOL [43].

antibacterial activity alike was tested considering *N. diversicolor* from which the native hedistin was originally isolated lives in estuary. Sodium chloride, to a final concentration of 300 mM, pH 5.2, was added to the above sample of hedistin either in water or in DPC environment, and then 2D NOESY spectra were recorded on the salted samples. The NOESY spectra of the salted samples shows extremely high similarity in both chemical shift values and NOE connectivity pattern with those corresponding spectra of the samples with no salt. Fig. S3 (supplementary data) shows all the unambiguous $d_{\alpha\beta}$ (i, i + 3) NOEs, Ala3/Ala6, Leu5/Lys8, Ala6/Val9, Val13/Tyr16, and Ala14/Ala17 in the NOESY spectrum for the high salted hedistin sample in DPC environment. This result means that the conformation of the synthesized hedistin either in water or in DPC environment is stable under the condition of up to 300 mM NaCl. Antibacterial activity test of this hedistin sample in high salt was also subsequently conducted showing that the activity of the synthesized hedistin does not change at high concentration salt (see supplementary material Table S2).

In summary, as viewed from the structure feature of hedistin, it could be classified into the family of cationic and amphipathic α-helical antimicrobial peptides containing a hinge in the middle showing much resemblance to LL-37 [60] in which there are 37 residues and a helical bend locating between residues Gly14 and Glu16 induces a kink in the middle of two amphipathic helices. Compared with other AMPs found mostly from hemocytes in invertebrates, hedistin, with its heterogeneous helix–turn–helix structure in DPC micelles displaying obvious amphipathic nature, is much like the antimicrobial peptides clavanins, styelins from ascidians [12,13]; it is far from tachyplesins, tachycitics and tachystatins found in horseshoe crab [10], and myticins and mytilins from mussels as well which generally form hairpin-like β-sheet motif and cysteine-stabilized α-β motif [9].

3.4. Molecular dynamics simulations

The above NMR and CD analysis has shown that hedistin exists as an amphipathic helix–turn–turn structure in DPC micelles while adopts a random coil configuration in aqueous solution. Both of the structure profiles are of rather static status of hedistin molecules that populated mainly among the lowest energy states in certain environments. In this work, we carried out molecular dynamics simulations for two systems. One is for hedistin in water environment, and the other is for peptide hedistin interaction with lipid membrane mimicked by POPC bilayers. The structure of peptide hedistin in DPC micelles determined using NMR techniques was used as the initial conformation of the simulations. Results of the molecular dynamic simulations are described in detail as follows.

3.4.1. The simulation of hedistin in water environment

The simulation of peptide in water was performed by solvating the hedistin molecule in a cubic box full of waters. Counter ions (Cl^-) were added to make the system electroneutral. The simulation was performed for 70 ns at 300 K. Fig. 10 shows a ribbon diagram of a representative structure of the initial and end of the 70 ns simulation (A), and the secondary structure of hedistin during the course of the simulation (B). As shown, α-helix content of the peptide becomes less and less and the secondary structure of the peptide incurs an obvious loss. This is because the water molecules compete hydrogen bond formation with the main chain of the peptide. The result of this simulation is completely consistent with the NMR and CD observations that the helical secondary structure can not stably exist in aqueous solution.

3.4.2. The simulation of hedistin at the POPC/water interface

Hedistin was placed in the water phase, close to the POPC/water interface but not disturbing the lipid head-group region, with the hydrophilic part of the amphipathic α-helix facing the lipid/water interface. Counter ions (Cl^-) were added to make the system electroneutral. The simulations were performed for 50 ns at 310 K and 363 K, respectively. Taking the simulation (1:128 peptide/lipid) at 310 K as example, Fig. 11 shows snapshots from the beginning, after 1, 6, 10 ns, and at the end of the simulation for the hedistin/lipid system. As shown, hedistin molecule, originally in the water phase, moves into the lipid environment and finally arrives at a position such that hydrophobic residues (Trp4, Leu5, Ala6, Val9, Ala17, Trp18)

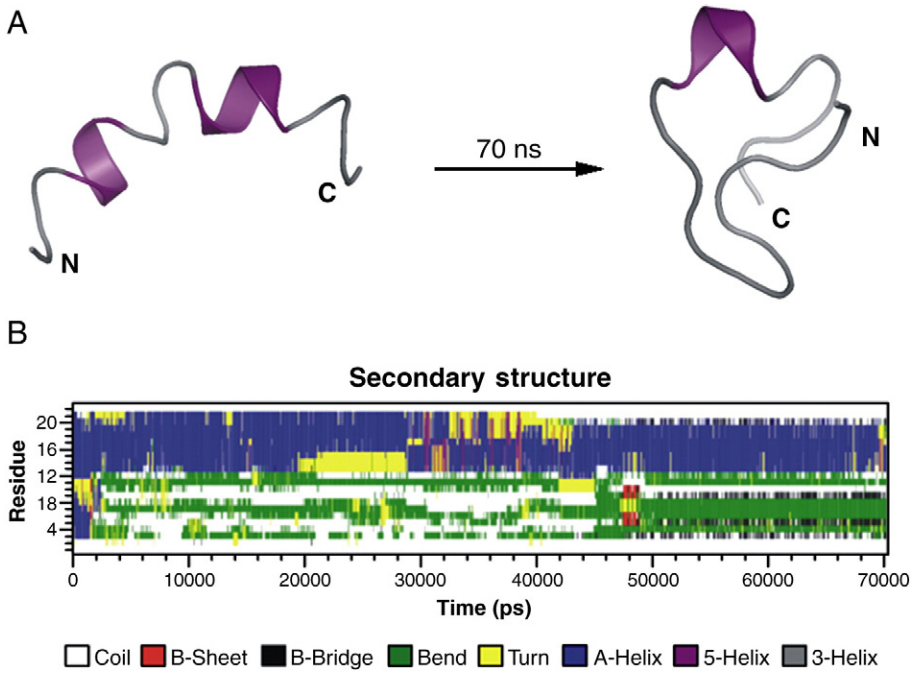

Fig. 10. Ribbon diagram of a representative structure of initial and end of 70 ns simulation with hedistin in water environment (A) and the secondary structure of hedistin during the course of the simulation (B) defined by DSSP algorithm (54). In panel B, The residue numbers run along the ordinate and simulation time along the abscissa. The secondary structure changes from a more helical starting condition to a distinct random structure.

interact with the lipid hydrophobic tail region and hydrophilic residues (especially Lys8 and Arg20 residues) interact with the lipid head-group region. The peptide rotates by about 180° during the entire simulation process. In more detail, the N-terminal region Leu1–Lys8 first arrives at the interface to interact with lipid head-groups seemingly driven mainly by Trp4 and Lys8 (Fig. 11) ($t=1$ ns), then, the side chains of the hydrophobic residues especially Trp4 with its large indole ring slowly permeate into the lipid hydrophobic tail region while the positively charged side chain of Lys8 still points to the head-group region and the inter-residue cation-π interaction between residues Trp4 and Lys8 is thus destroyed. In the mean time, the bend region Val9–Thr12 and the second helix Thr15–Tyr21 still stay in the water phase (Fig. 11) ($t=1$–6 ns). After ~6 ns simulation, the second helix begins to insert into the lipid phase seemingly driven mainly by Trp18 and Arg20. Noticeably, the bend region remains at the water/lipid interface almost throughout the process (Fig. 11) ($t=6$–50 ns). At the temperature of 363 K, a prominently discrete behavior for the three segments of the peptide was also found in the 50 ns MD simulation in that the second helix this time, prior to the first helical segment, binds to the lipid head-group region and subsequently permeates into the hydrophobic lipid tail region, while the hinge remains the last portion entering lipid environment. We also carried out simulations at a higher concentration ratio of peptide to lipid, i.e. five peptide molecules were placed on the surface of lipid membrane of 128 molecules at the beginning, and obtained rather similar results (data not shown) showing this kind of in-segments dynamical feature of hedistin.

In all simulations performed here (1:128 peptide/lipids at both 310 K and 363 K, or 5:128 peptides/lipids at 310 K), no simultaneous entering to the lipid membrane environment was observed for two of the three segments of the heterogeneous helix–turn–helix molecule, which we herein term as dynamical heterogeneity of the helix–turn–helix structure. This observation has been further verified by more simulations in which rather a few random ways of placing hedistin molecule on the bilayer surface were tested. Good repeatability of this in-segments behavior in the early stage of MD simulation of hedistin-POPC interaction was obtained as long as the peptide was placed with no segment in preference to the others, i.e. letting the molecule plane parallel the bilayer surface. This dynamical heterogeneity characteristic of hedistin seems attributed to the structural heterogeneity of hedistin, and could be reasonably explained via analyses of hydrogen bond formation and the hydrophobicity of each of the three segments.

3.4.3. Hydrogen bond analysis of the peptide-POPC system

The lipid tail region is devoid of charges and is highly hydrophobic. On the other hand, the lipid head-group region, consisting of the phosphate, glycerol and choline groups, is a complex domain where electrostatic interactions are likely to dominate. The oxygen atoms in the glycerol and phosphate groups are likely to interact favorably with the positively charged groups of the peptides, and could lead to hydrogen bonding between the peptides and the lipid head-groups. We performed a hydrogen bond analysis of peptide–lipid and peptide–water pairs in the entire simulation at 310 K for the ensemble with peptide/lipid ratio of 1:128. The conditions $r \leq 0.35$ nm and $\alpha \leq 60°$ were used as criteria for a hydrogen bond (H-bond) to exist (a hydrogen bond was assumed to exist if the donor-acceptor distance is not more than 0.35 nm and the angle of donor-hydrogen-acceptor triplet is not more than 60°). The total number of hydrogen bonds between the peptide–water, peptide–lipid pairs during the entire 50 ns simulation is shown in Fig. 12. As shown, the number of the peptide–water hydrogen bonds is decreasing, whereas the number of the peptide–lipid hydrogen bonds is correspondingly increasing as a function of time, implying the peptide is moving into lipid bilayers from water phase to interact with lipid bilayers.

Fig. 13 shows the hydrogen bond existence map for a few typical residues bonding with POPC bilayers. Residues Trp4 forms hydrogen bonds with the lipid head-group region during the early 16 ns and no longer after that (Fig. 13A). Residue Lys8 forms stable hydrogen bonds with the lipid head-group region through the whole 50 ns simulation (Fig. 13B). Residues Trp18 forms stable hydrogen bonds between 6–18 ns (Fig. 13C) and Asn19 after 6 ns (data not shown). Residue Arg20 forms persistent hydrogen bonds between 12 and 30 ns (data not shown). Tyr21 forms hydrogen bond after 6 ns (Fig. 13D). From the y axis value–hydrogen bond index (each hydrogen bond index refers to a unique donor-hydrogen-acceptor triplet), we observed that hydrogen bonds of residues Lys8 and Arg20 are mainly from the side chain ammonium group (NH_3^+) and guanidine, respectively, and the number of hydrogen bonds of residue Arg20 is much more than that of residue Lys8 since arginine contains more hydrogen bond donors. Residue Thr15 forms stable hydrogen bonds with the lipid head-group region only after approximately 21 ns (Fig. 13E), similar results happened to residues Thr12 and Tyr16 that also fall in or very near the hinge region (data not shown). In all, the above hydrogen bond analyses imply that the first helical region containing residues Trp4 and Lys8 is the first part that starts to contact the lipid head-group region via hydrogen bonding, followed by the second α-helix including residues Trp18, Asn19 and Arg20. Residues Thr12, Thr15 and Tyr16 in or near the hinge region only form hydrogen bonds with the lipid head-group region in the end of the simulation. This hydrogen bond analysis quantitatively confirms the dynamical heterogeneity characteristic of the helix–turn–helix motif of hedistin.

Both tryptophan residues Trp4 and Trp18 were found not only to present an obvious preference for the lipid head-group region of bilayers to the water phase but also playing a key role in driving

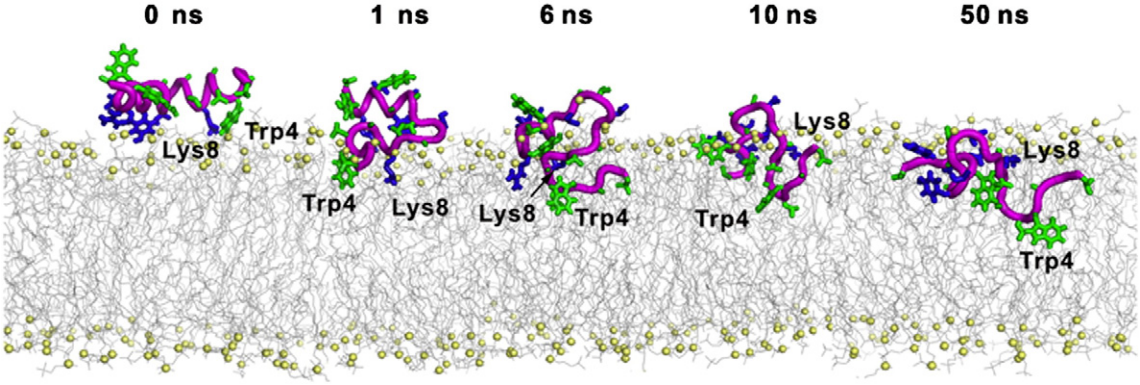

Fig. 11. Snapshots from the beginning, after 1, 6, 10 ns, and at the end of the 50 ns simulation of 1:128 hedistin/POPC system at 310 K. In each case, the side chains of the hydrophilic residues are shown in blue and the hydrophobic residues in green. POPC lipid bilayers are shown in grey except that the phosphorus atoms of lipid head-groups are shown in pale-yellow spheres. The backbone of peptide hedistin is shown in magenta tube. The water molecules have been removed for sake of clarity.

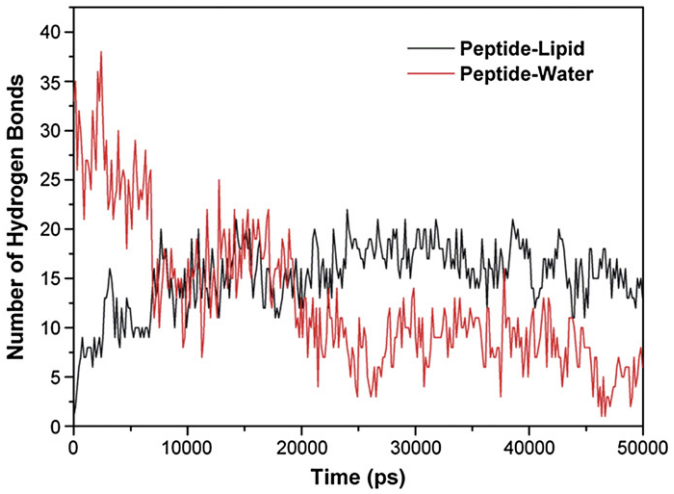

Fig. 12. Total number of hydrogen bonds between the peptide–water (—), peptide–lipid (—) pairs during the whole 50 ns simulation of hedistin at the POPC/water interface. A trend of increasing lipid-peptide hydrogen bonds and a reduction in peptide–water hydrogen bonds was observed.

peptide to bury deeper into the hydrocarbon core of lipid bilayers, which is supported by the hydrogen bond existence map of residues Trp4 and Trp18. Residue Trp4 in the first helix forms hydrogen bonds with the lipid head-group region only in the first 16 ns and no longer after that, and residue Trp18 in the second helix also presents a similar behavior (Fig. 13A and C), implying that residues Trp4 and Trp18 form hydrogen bonds with the lipid head-group region just when residing in the interfacial region, but they have permeated into deeper hydrocarbon core of lipid bilayers after that. On the contrary, as lack of residues with preference for membrane interface like tryptophan and residues effectively attracting peptide from water phase to the target membrane like lysine and arginine, the hinge segment of hedistin, turns out to be the final part to enter the lipid environment.

We also observed obvious loss of the secondary structure of hedistin in all of the simulations. This could be attributed to the lack of charged residues in hedistin, which may lead to the backbone of helix exposed to lipid molecules, resulting in destruction of the intra-helix hydrogen bonds. Similar phenomenon was observed in a 20 ns simulation of antimicrobial peptides maganin2 with POPC lipid bilayers [51].

4. Discussion

The three-dimensional structure of hedistin in aqueous solution and DPC micelles was carefully examined and the dynamical process of the peptide interaction with mimetic lipid membrane was simulated in this study. Hedistin was found to exist in a disordered state in water and in phosphate buffer, but α-helix dominating conformations appear when it is in SDS and DPC environment. The structure in DPC was demonstrated to be amphipathic and consisted of three segments forming a helix–bend–helix motif. The heterogeneity of the helix–turn–helix structure was then found to be corresponding to its dynamical heterogeneity at the early stage (0–50 ns) in molecular dynamics simulations of the peptide interaction with mimetic lipid membrane. The corresponding heterogeneous nature in its structure and dynamics reflects itself in that, the first N-terminal helical segment, prior to or following (at different temperature) the second helix, binds to the lipid head-group region and subsequently permeates into the hydrophobic lipid tail region, and the hinge is the last portion entering the lipid environment. The presence/absence of tryptophan, lysine and arginine residues is most likely responsible for the dynamical heterogeneity of hedistin.

The helix–turn–helix or helix–bend–helix structural motif has been observed in a variety of AMPs [60–64] as well as in other functional proteins [65]. With a common feature of having a hinge or kink between two helical segments, these AMPs can be roughly classified into two groups according to the residue composition of the turn motif, one is that the hinge is induced mainly by proline residue and the other, mainly by glysine residue. Caerin1.1 and maculatin 1.1

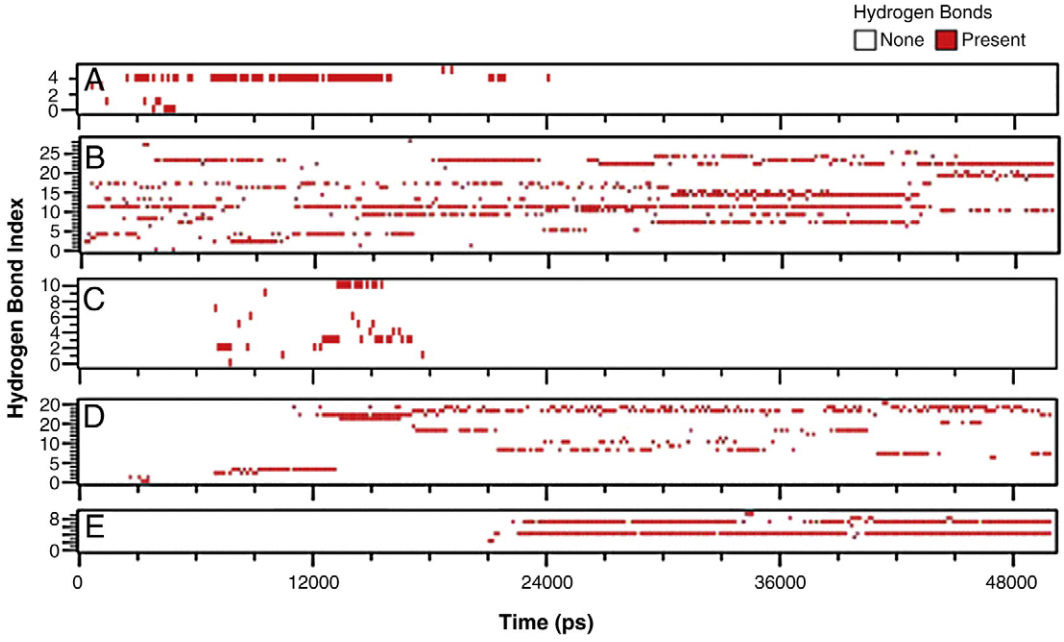

Fig. 13. Hydrogen bond existence map for residues (A) Trp4, (B) Lys8, (C) Trp18, (D) Tyr21 and (E) Thr15 of peptide hedistin with POPC lipid bilayers during the whole 50 ns simulation of hedistin at the POPC/water interface. The hydrogen bond indices run along the ordinate and simulation time along the abscissa. Each hydrogen bond index refers to a unique donor–hydrogen–acceptor triplet. Red lines show the presence of a hydrogen bond at that specific time.

from Australian green tree frogs and the Cecropin family from insect hemolymph belong to the former class, and hedistin and LL-37 belong to the latter [60–63]. Ranatuerin-2CSa is a most recently identified antibacterial peptide possessing helix–turn–helix structure with a turn formed by four residues Leu22, Glu23, Thr24, and Leu25 in its 30 residues long sequence [64].

A few experiments have been performed on the effect of the turn motif in the antibacterial activity of these AMPs. Mutation from proline residues to glysine or alanine residues decreases the flexibility and activity of Caerin1.1, proving that the flexible hinge formed around proline residues is critical to an optimal orientation between N- and C-terminal alpha helices when the peptide interacts with bacterial cell membranes [66]. The kink produced by Pro14 in gaegurin-6 was assumed to be important in bacterial cell lysis [67]. However, to our best knowledge, the detailed mechanism of the turn motif action underlying these experimental observations has not been carefully examined. In this study, our molecular dynamics simulations of hedistin interaction with mimetic membrane links the heterogeneous helix–bend–helix structural characteristics of hedistin to its dynamical heterogeneity at the early stage (covering 50 ns) of its antibacterial function process. The observation that the hinge region is the last portion entering the lipid environment probably acts as an important factor influencing its antibacterial activity. Furthermore, this result lends support to the "carpet" model of hedistin action as it could be hard for the whole molecule to traverse or translocate to the other side of the membrane due to the impeding effect of the hinge region. As rather a few AMPs have been demonstrated to consist of a helix–turn–helix structure, we could speculate that the dynamics behavior of such AMPs is likely to show similar segmental heterogeneity in light of their structural heterogeneity basis, and this characteristic of early stage dynamics may result in a corresponding way of disrupting the bacterial membrane.

The antimicrobial action is presumed to occur at microsecond or millisecond time-scales. So, 50 ns simulation is only for the early stage of the antimicrobial action process. Moreover, zwitterionic lipid POPC employed in the stated simulations is no longer the best feasible model of bacterial membrane thanks to the rapid development of this area [68,69]. Therefore, larger time scale simulations (up to hundreds of nanosecond) of hedistin interaction with phosphatidylethanolamine (PE), phosphatidylglycerol (PG), and mixed PE and PG lipids are ongoing and expected to give rise to more interesting results in view of PE and PG constituting the main lipid components of bacterial membranes. In addition, if the conformation and dynamics results obtained for the synthesized hedistin devoid of bromines apply to the native hedistin possessing bromotryptophan residues still needs to investigate since the influence of bromines on the structure has not been verified although Tasiemski et al. [14] determined the presence of bromines in the native hedistin.

Acknowledgements

The authors greatly appreciate financial support from the National Natural Science Foundation of China (#20475019).

Appendix A. Supplementary data

Supplementary data associated with this article can be found, in the online version, at doi:10.1016/j.bbamem.2009.10.001.

References

[1] R.E.W. Hancock, R. Lehrer, Cationic peptides: a new source of antibiotics, Trends Biotechnol. 16 (1998) 82–88.
[2] L. Marri, R. Dallai, D. Marchini, The novel antibacterial peptide ceratotoxin A alters permeability of the inner and outer membrane of Escherichia coli K-12, Curr. Microbiol. 33 (1996) 40–43.
[3] R.E.W. Hancock, Cationic antimicrobial peptides: towards clinical applications, Expert Opin. Invest. Drugs 9 (2000) 1723–1729.
[4] S.K. Fridkin, D.S. Yokoe, C.G. Whitney, A. Onderdonk, D.C. Hooper, Epidemiology of a dominant clonal strain of vancomycin-resistant Enterococcus faecium at separate hospitals in Boston, Massachusetts, J. Clin. Microbiol. 36 (1998) 965–970.
[5] C.J. Donskey, J.R. Schreiber, M.R. Jacobs, R. Shekar, R.A. Salata, S. Gordon, C.C. Whalen, F. Smith, L.B. Rice, A polyclonal outbreak of predominantly VanB vancomycin-resistant enterococci in northeast Ohio. Northeast Ohio Vancomycin-Resistant Enterococcus Surveillance Program, Clin. Infect. Dis. 29 (1999) 573–579.
[6] P.A. Maple, J.M. Hamilton-Miller, W. Brumfitt, World-wide antibiotic resistance in methicillin-resistant *Staphylococcus aureus*, Lancet 11 (1989) 537–540.
[7] M.A. Martin, Methicillin-resistant *Staphylococcus aureus*: the persistent resistant nosocomial pathogen, Curr. Clin. Top. Infect. Dis. 14 (1994) 170–191.
[8] R. Medzhitov, C.J. Janeway, Innate immune recognition: mechanisms and pathways, Immunol. Rev. 173 (2000) 89–97.
[9] G. Mitta, F. Vandenbulcke, P. Roch, Original involvement of antimicrobial peptides in mussel innate immunity, FEBS Lett. 486 (2000) 185–190.
[10] S. Iwanaga, The molecular basis of innate immunity in the horseshoe crab, Curr. Opin. Immunol. 14 (2002) 87–95.
[11] E. Bachere, Y. Gueguen, M. Gonzalez, J. de Lorgeril, J. Garnier, B. Romestand, Insights into the anti-microbial defense of marine invertebrates: the penaeid shrimps and the oyster Crassostrea gigas, Immunol. Rev. 198 (2004) 149–168.
[12] I.H. Lee, C. Zhao, Y. Cho, S.S. Harwig, E.L. Cooper, R.I. Lehrer, Clavanins, alpha-helical antimicrobial peptides from tunicate hemocytes, FEBS Lett. 400 (1997) 158–162.
[13] I.H. Lee, Y.S. Lee, C.H. Kim, C.R. Kim, T. Hong, L. Menzel, L.M. Boo, J. Pohl, M.A. Sherman, A. Waring, R.I Lehrer, Dicynthaurin: an antimicrobial peptide from hemocytes of the solitary tunicate, *Halocynthia aurantium*, Biochim. Biophys. Acta 1527 (2001) 141–148.
[14] A. Tasiemski, D. Schikorski, F. Le Marrec-Croq, C. Pontoire-Van Camp, C. Boidin-Wichlacz, P.E. Sautière, Hedistin, a novel antimicrobial peptide containing bromotryptophan constitutively expressed in the NK cells-like of the marine annelid, *Nereis diversicolor*, Dev. Comp. Immunol. 31 (2007) 749–762.
[15] M. Solé, J. Kopecka-Pilarczyk, J. Blasco, Pollution biomarkers in two estuarine invertebrates, *Nereis diversicolor* and *Scrobicularia plana*, from a Marsh ecosystem in SW Spain, Environ. Int. 35 (2009) 523–531.
[16] D.P. Tieleman, S.J. Marrink, Lipids out of equilibrium: energetics of desorption and pore mediated flip-flop, J. Am. Chem. Soc. 128 (2006) 12462–12467.
[17] R.W. Pastor, R.M. Venable, S.E. Feller, Lipid bilayers, NMR relaxation, and computer simulations, Acc. Chem. Res. 35 (2002) 438–446.
[18] M.B. Ulmschneider, D.P Tieleman, M.S. Sansom, The role of extra-membranous inter-helical loops in helix–helix interactions, Protein Eng. Des. Sel. 18 (2005) 563–570.
[19] J.B. Klauda, N. Kucerka, B.R. Brooks, R.W. Pastor, J.F. Nagle, Simulation-based methods for interpreting x-ray data from lipid bilayers, Biophys. J. 90 (2006) 2796–2807.
[20] D. Wade, A. Boman, B. Wahlin, C.M. Drain, D. Andreu, H.G. Boman, R.B. Merrifield, All-D amino acid-containing channel-forming antibiotic peptides, Proc. Natl. Acad. Sci. U. S. A. 87 (1990) 4761–4765.
[21] R. Bessalle, A. Kapitkovsky, A. Gorea, I. Shalit, M. Fridkin, All-D-magainin: chirality, antimicrobial activity and proteolytic resistance, FEBS Lett. 274 (1990) 151–155.
[22] E.L. Merrifield, S.A. Mitchell, J. Ubach, H.G. Boman, D. Andreu, R.B. Merrifield, D-enantiomers of 15-residue cecropin A-melittin hybrids, Int. J. Pept. Protein Res. 46 (1995) 214–220.
[23] S.J. Ludtke, K. He, W.T. Heller, T.A. Harroun, L. Yang, H.W. Huang, Membrane pores induced by magainin, Biochemistry 35 (1996) 13723–13728.
[24] K. Matsuzaki, O. Murase, N. Fujii, K. Miyajima, An antimicrobial peptide, magainin 2, induced rapid flip-flop of phospholipids coupled with pore formation and peptide translocation, Biochemistry 35 (1996) 11361–11368.
[25] E. Gazit, A. Boman, H.G. Boman, Y. Shai, Interaction of the mammalian antibacterial peptide cecropin P1 with phospholipid vesicles, Biochemistry 34 (1995) 11479–11488.
[26] Y. Pouny, D. Rapaport, A. Mor, P. Nicolas, Y. Shai, Interaction of antimicrobial dermaseptin and its fluorescently labeled analogs with phospholipid membranes, Biochemistry 31 (1992) 12416–12423.
[27] G. Choi, J. Guo, A. Makriyannis, The conformation of the cytoplasmic helix 8 of the CB1 cannabinoid receptor using NMR and circular dichroism, Biochim. Biophys. Acta 1668 (2005) 1–9.
[28] C. Perez, M. Paul, P. Bazerque, An antibiotic assay by the agar well diffusion method, Acta Biol. Med. Exp. 15 (1990) 113–115.
[29] L. Braunschweiler, R.R. Ernst, Coherence transfer by isotropic mixing; application to proton correlation spectroscopy, J. Magn. Reson. 53 (1983) 521–528.
[30] M. Rance, O.W. Sorensen, G. Bodenhausen, G. Wagner, R.R. Ernst, K. Wüthrich, Improved spectral resolution in COSY ^{1}HNMR spectra of proteins via double quantum filtering, Biochem. Biophys. Res. Commun. 117 (1983) 479–485.
[31] A. Kumar, R.R. Ernst, K. Wüthrich, A two-dimensional nuclear Overhauser enhancement, (2D NOE) experiment for the elucidation of complete proton–proton cross-relaxation networks in biological macromolecules, Biochem. Biophys. Res. Commun. 95 (1980) 1–6.
[32] D. Marion, M. Ikura, R. Tschudin, A. Bax, Rapid recording of 2D NMR spectra without phase cycling. Application to the study of hydrogen exchange in proteins, J. Magn. Reson. 85 (1989) 393–399.
[33] M. Piotto, V. Saudek, V. Sklenar, Gradient-tailored excitation for single-quantum NMR spectroscopy of aqueous solutions, J. Biomol. NMR 2 (1992) 661–665.
[34] S.H. Smallcomb, S.L. Patt, P.A. Keifer, WET solvent suppression and its applications to LC NMR and high-resolution NMR spectroscopy, J. Magn. Reson. Ser. A 117 (1995) 295–303.
[35] A. Bax, D.G. Davis, MLEV-17 based two-dimensional homonuclear magnetization transfer spectroscopy, J. Magn. Reson. 65 (1985) 355–360.

[36] F. Delaglio, S. Grzesiek, G.W. Vuister, G. Zhu, J. Pfeifer, A. Bax, NMRPipe: a multidimensional spectral processing system based on UNIX pipes, J. Biomol. NMR 6 (1995) 277–293.
[37] T. D. Goddard, D. G. Kneller, SPARKY 3, University of California, San Francisco.
[38] G.M. Clore, A.M. Gronenborn, Determination of three-dimensional structures of proteins and nucleic acids in solution by nuclear magnetic resonance spectroscopy, Crit. Rev. Biochem. Mol. Biol. 24 (1989) 479–564.
[39] K. Wüthrich, M. Billeter, W. Braun, Pseudo-structures for the 20 common amino acids for use in studies of protein conformations by measurements of intramolecular proton-proton distance constraints with nuclear magnetic resonance, J. Mol. Biol. 169 (1983) 949–961.
[40] G.M. Clore, A.M. Gronenborn, M. Nilges, C.A. Ryan, Three-dimensional structure of potato carboxypeptidase inhibitor in solution. A study using nuclear magnetic resonance, distance geometry, and restrained molecular dynamics, Biochemistry 26 (1987) 8012–8023.
[41] A.T. Brünger, P.D. Adams, G.M. Clore, W.L. Delano, P. Gros, R.W. Grosse-Kunstleve, J.S. Jiang, J. Kuszewski, M. Nilges, N.S. Pannu, R.J. Read, L.M. Rice, T. Simonson, G.L. Warren, Crystallography and NMR system: a new software suit for macromolecular structure determination, Acta Crystallogr., Sect. D: Biol. Crystallogr. 54 (1998) 905–921.
[42] R. Koradi, M. Billeter, K. Wüthrich, MOLMOL: a program for display and analysis of macromolecular structure, J. Mol. Graph. 14 (1996) 51–55.
[43] W.L. DeLano, The PyMOL Molecular Graphics System, DeLano Scientific, San Carlos, CA, USA (http://www.pymol.org), 2002.
[44] R. Laskowski, M. MacArthur, D. Moss, J. Thornton, PROCHECK: a program to check the stereochemical quality of protein structures, J. Appl. Cryst. 26 (1993) 283–291.
[45] E. Lindahl, B. Hess, D. van der Spoel, GROMACS 3.0: a package for molecular simulation and trajectory analysis, J. Mol. Model 7 (2001) 306–317.
[46] D.P. Tieleman, M.S.P. Sansom, H.J.C. Berendsen, An alamethicin channel in a lipid bilayer: molecular dynamics simulation, Biophys. J. 76 (1999) 1757–1769.
[47] B. Hess, H. Bekker, H.J.C. Berendsen, J.G.E.M. Fraaije, LINCS: a linear constraint solver for molecular simulations, J. Comp. Chem. 18 (1997) 1463–1472.
[48] U. Essmann, L. Perera, M.L. Berkowitz, T. Darden, H. Lee, L.G. Pedersen, A smooth particle mesh Ewald method, J. Chem. Phys. 103 (1995) 8577–8593.
[49] W. Humphrey, A. Dalke, K. Schulten, VMD: visual molecular dynamics, J. Mol. Graphics 14 (1996) 33–38.
[50] H.J.C. Berendsen, J.P.M. Postma, W.F. van Gunsteren, A. Dinola, J.R. Haak, Molecular dynamics with coupling to an external bath, J. Chem. Phys. 81 (1984) 3684–3690.
[51] S.K. Kandasamy, R.G. Larson, Binding and insertion of alpha-helical anti-microbial peptides in POPC bilayers studied by molecular dynamics simulations, Chem. Phys. lipids 132 (2004) 113–132.
[52] K. Wüthrich, NMR of protein and nucleic acid, Wiley, New York, 1986.
[53] D.S. Wishart, B.D. Sykes, F.M. Richards, The chemical shift index: a fast and simple method for the assignment of protein secondary structure through NMR spectroscopy, Biochemistry 31 (1992) 1647–1651.
[54] W. Kabsch, C. Sander, Dictionary of protein secondary structure: pattern recognition of hydrogen-bonded and geometrical features, Biopolymers 22 (1983) 2577–2637.
[55] H.L.J. Wienk, M. Czisch, B. Kruijff, The structural flexibility of the preferredoxin transit peptide, FEBS Lett. 453 (1999) 318–326.
[56] V. Wray, D. Mertins, M. Kiess, P. Henklein, W. Trowizsch-Kienast, U. Schubert, Solution structure of the cytoplasmic domain of the human CD4 glycoprotein by CD and ^{1}H NMR spectroscopy: implications for biological functions, Biochemistry 37 (1998) 8527–8538.
[57] G.E. Gilbert, J.D. Baleja, Membrane-binding peptide from the C2 domain of factor VIII forms an amphipathic structure as determined by NMR spectroscopy, Biochemistry 34 (1995) 3022–3031.
[58] P.B. Crowley, A. Golovin, Cation-pi interactions in protein–protein interfaces, Proteins 59 (2005) 231–239.
[59] H. Khandelia, Y.N. Kaznessis, Cation-pi interactions stabilize the structure of the antimicrobial peptide indolicidin near membranes: molecular dynamics simulations, J. Phys. Chem. B. 111 (2007) 242–250.
[60] G.S. Wang, Structures of human host defense cathelicidin LL-37 and its smallest antimicrobial peptide KR-12 in lipid micelles, J. Biol. Chem. 283 (2008) 32637–32643.
[61] H. Wong, J.H. Bowie, J.A. Carver, The solution structure and activity of caerin 1.1, an antimicrobial peptide from the Australian green tree frog, Litoria spzendida, Eur. J. Biochem. 247 (1997) 545–557.
[62] B.C. Chia, J.A. Carver, T.D. Mulhern, J.H. Bowie, Maculatin 1.1, an anti-microbial peptide from the Australian tree frog, Litoria genimaculata solution structure and biological activity, Eur. J. Biochem. 267 (2000) 1894–1908.
[63] T.A. Holak, A. Engström, P.J. Kraulis, G. Lindeberg, H. Bennich, T.A. Jones, A.M. Gronenborn, G.M. Clore, The solution conformation of the antibacterial peptide cecropin A: a nuclear magnetic resonance and dynamical simulated annealing study, Biochemistry 27 (1988) 7620–7629.
[64] A.P. Subasinghage, J.M. Conlon, C.M. Hewage, Conformational analysis of the broad-spectrum antibacterial peptide, ranatuerin-2CSa: identification of a full length helix–turn–helix motif, Biochim. Biophys. Acta 1784 (2008) 924–929.
[65] W.D. Kohn, C.T. Mant, R.S. Hodges, α-helical protein assembly motifs, J. Biol. Chem 272 (1997) 2583–2586.
[66] T.L. Pukala, C.S. Brinkworth, J.A. Carver, J.H. Bowie, Investigating the importance of the flexible hinge in caerin 1.1: solution structures and activity of two synthetically modified caerin peptides, Biochemistry 43 (2004) 937–944.
[67] J.Y. Suh, K.H. Lee, S.W. Chi, S.Y. Hong, B.W. Choi, H.M. Moon, B.S. Choi, Unusually stable helical kink in the antimicrobial peptide-a derivative of gaegurin, FEBS Lett. 392 (1996) 309–312.
[68] E. Mátyus, C. Kandt, D.P. Tieleman, Computer simulation of antimicrobial peptides, Curr. Med. Chem. 14 (2007) 2789–2798.
[69] D.E. Elmore, Molecular dynamics simulation of phosphatidylglycerol membrane, FEBS Lett. 580 (2006) 144–148.